

# PCCP

Accepted Manuscript



This is an *Accepted Manuscript*, which has been through the Royal Society of Chemistry peer review process and has been accepted for publication.

*Accepted Manuscripts* are published online shortly after acceptance, before technical editing, formatting and proof reading. Using this free service, authors can make their results available to the community, in citable form, before we publish the edited article. We will replace this *Accepted Manuscript* with the edited and formatted *Advance Article* as soon as it is available.

You can find more information about *Accepted Manuscripts* in the [Information for Authors](#).

Please note that technical editing may introduce minor changes to the text and/or graphics, which may alter content. The journal's standard [Terms & Conditions](#) and the [Ethical guidelines](#) still apply. In no event shall the Royal Society of Chemistry be held responsible for any errors or omissions in this *Accepted Manuscript* or any consequences arising from the use of any information it contains.

# Aqueous solvation of HgClOH. Stepwise DFT solvation and Born-Oppenheimer Molecular Dynamics studies of the HgClOH-(H<sub>2</sub>O)<sub>24</sub> complex.

J.I. Amaro-Estrada<sup>a</sup>, L. Maron<sup>b</sup> and A. Ramírez-Solís<sup>b\*</sup>

<sup>a</sup> Departamento de Física, Facultad de Ciencias. Universidad Autónoma del Estado de Morelos. Av. Universidad 1001. Cuernavaca, Morelos. 62209, México.

<sup>b</sup> Université de Toulouse, INSA Laboratoire de Physicochimie de Nano-Objets, 135 Avenue de Rangueil, F31077 Toulouse, France.

## Abstract

We address the aqueous solvation of HgClOH through a systematic study of stepwise hydration considering the HgClOH-(H<sub>2</sub>O)<sub>*n*</sub> structures with *n* = 1-24. After calibration of the DFT method, the electronic calculations have been carried out using the B3PW91 exchange-correlation functional. For *n*<5 the main geometrical parameters and incremental binding energies are in agreement with counterpoise-corrected MP2/AVTZ static values and BO-MP2 dynamic averages. For *n*>15 three direct water-Hg interactions appear during the hydration process and a pentacoordinated trigonal bipyramid apical pattern around Hg is found. 22 water molecules are needed to build the first solvation shell. Unlike microsolvated HgCl<sub>2</sub>, no stable equatorial trigonal bipyramid was found. Optimizations with the Polarizable Continuum Model lead to structures with extremely large Hg-O(water) distances because of a dominant solvation effect on the explicit water molecules; however this overestimation diminishes for large values of *n*. A DFT Born-Oppenheimer molecular dynamics simulation at T=700 K revealed the stability of the HgClOH-(H<sub>2</sub>O)<sub>24</sub> complex with an average trigonal bipyramid Hg-coordination pattern, in accordance with the static cluster description. After thermalization is achieved, the exchange rate for the Hg-coordinated water molecules is estimated ca. 10<sup>11</sup> s<sup>-1</sup>.

\*On sabbatical leave from Facultad de Ciencias, Universidad Autónoma del Estado de Morelos.

e-mail: [alex@uaem.mx](mailto:alex@uaem.mx)

## I. Introduction

Due to the extensive global industrial activity in the last 160 years, the concentration of Hg levels in ecosystems worldwide has increased significantly. In particular, surface soils and aquatic environments [1] have accumulated high levels of this toxic metal even in remote regions such as the Arctic [2]. From the ecological point of view it is crucial to find relevant information on the fate, transport and pathways of mercury species in these biological environments. It is difficult to establish the exact amount of mercury worldwide, however approximately 90% of Hg in the atmosphere has been found as elemental Hg(0), although the ratio of free monatomic vapor varies continually [3,4] due to oxidation processes to Hg<sup>2+</sup> forms that occur through various physical and chemical mechanisms. Many adverse effects of Hg accumulation in humans are well known, particularly on the nervous and immune systems. One of the most important entrance pathways of mercury complexes into the food chain is through photosynthetic organisms and bacteria, which are then ingested by higher predators (marine mammals, fish, polar bears, seabirds, etc.) leading to a process of mercury accumulation and biomagnification. Previous studies about the bioaccumulation [5] and methylation [6] processes of mercury have shown that HgCl<sub>2</sub>, HgClOH and Hg(OH)<sub>2</sub> are the most abundant Hg-containing inorganic complexes in aqueous environments.

The bioavailability of deposited mercury is followed by a crucial biochemical step in which one or several Hg-containing species cross the cell membrane by passive or active diffusion. However, this kind of process is dependent on the specific type of ligands bonded to the Hg atom. Gutknecht [7] and Myers *et al.* [8] compared the permeability rates of several Hg-ligand complexes across laboratory-synthesized lipid bilayer membranes. Both studies found that lipid membranes are highly permeable to HgCl<sub>2</sub>, Hg(OH)<sub>2</sub> and HgClOH.

Since we have performed previous studies concerning the aqueous solvation of Hg(OH)<sub>2</sub> [9] and HgCl<sub>2</sub> [10], in this work we report a detailed study the main structural and energetic features of the stepwise hydration of HgClOH. Once we reach the formation of the first

solvation shell, we include the temperature effects on the system through DFT Born-Oppenheimer molecular dynamics simulations. The study of the intra and inter-molecular interactions using a cluster description of the aqueous solvation of Hg-containing molecules is the first step to reach a more realistic description through Monte Carlo simulations of the condensed phase. Recently, this MC approach was used by some of us to accurately describe aqueous solvation of  $\text{As}(\text{OH})_3$  [11] and  $\text{HgCl}_2$  [12] in the liquid phase. Based on an adequate description of the microsolvated species in the gas phase, the next stage in our research is the development of refined interatomic interaction potentials needed to carry out classical Monte Carlo simulations of  $\text{HgClOH}$  in aqueous solution as we have done for the  $\text{HgCl}_2$  molecule [12].

## II. Method and Computational details

### A. Calibration of the method

A systematic study by stepwise hydration of  $\text{HgClOH}$  was carried out at the DFT level, i.e., water molecules were added to previously optimized  $\text{HgClOH}-(\text{H}_2\text{O})_n$  structures until the first solvation shell was fully formed. Incremental water binding energies and optimized structures have been computed. As in our previous studies the Hg and Cl atoms [14,15] were treated with the Stuttgart-Köln relativistic effective core potentials in combination with their adapted valence basis sets, augmented by a set of polarization functions previously reported in ref. [16]. The Dunning *aug-cc-pVTZ* (AVTZ) [13] basis sets for the oxygen and hydrogen atoms were used for  $n < 5$ . Since calculations with the AVTZ basis already lead to 506 molecular orbitals for the  $\text{HgClOH}-(\text{H}_2\text{O})_4$  pentamer, for the systematic microsolvation study involving a larger number of water molecules the 6-311G(d,p) basis sets for O and H were utilized.

As a first step we have verified that single reference methods, such as the MP2 approach, are

well adapted to describe accurately the stepwise solvation process. In order to do so, using the CCSD/cc-pVTZ method we have obtained the T1Diagnostic for the smaller HgClOH-(H<sub>2</sub>O)<sub>n</sub> systems (n=0,1, and 2) at their optimized MP2 geometries. As could be expected, in all cases the T1Diagnostic was found to be quite small (T1Diag<0.0128). These results are in agreement with the previous report by Shepler *et al.* [17] where they used the MP2 and B3LYP methods to study the microsolvation of several mercury-mono and -dihalide species. Thus, as in our previous microsolvation studies of HgCl<sub>2</sub> and Hg(OH)<sub>2</sub>, the MP2 method provides reliable structural and energetic references. Secondly, in order to determine the exchange-correlation functional to be used we have performed a careful calibration using as reference the MP2/aug-cc-pVTZ(AVTZ) results for the HgClOH-(H<sub>2</sub>O)<sub>n</sub> systems with n=0,1 and 2. This calibration involved three aspects: optimized geometrical parameters, harmonic vibrational frequencies and incremental solvation energies. Table 1 shows the comparison of the structural results obtained with some representative functionals vs. the MP2 values, while Table 2 shows the comparison of the incremental water binding energies (WBE). The vibrational spectra obtained at the MP2 level and with the various exchange-correlation functionals are given as Supplementary Material.

**Table 1.** Calibration of the method: comparison of optimized geometrical parameters of HgClOH-(H<sub>2</sub>O)<sub>n</sub> (n=1-2) complexes with various functionals with the MP2 references. The O<sub>w</sub> stands for the water oxygen atoms directly linked to Hg. Distances in Å, angles in degrees.

<i>n</i>	Level	Hg-Cl	Hg-O(H)	Cl-Hg-O(H)	Hg-O <sub>w</sub>
0	B3LYP/AVTZ	2.33	1.99	176.9	
	B971/AVTZ	2.32	1.98	176.9	
	PBE0/AVTZ	2.30	1.97	177.0	
	M06/AVTZ	2.32	1.98	177.0	

	B3PW91/AVTZ	2.31	1.97	177.0	
	MP2/AVTZ	2.30 <sup>a</sup>	1.94 <sup>a</sup>	176.5 <sup>a</sup>	
1	B3LYP/AVTZ	2.33	2.01	179.8	2.83
	B971/AVTZ	2.32	2.00	179.8	2.84
	PBE0/AVTZ	2.31	1.99	179.6	2.78
	M06/AVTZ	2.32	2.01	179.5	2.72
	B3PW91/AVTZ	2.31	1.99	177.0	2.82
	MP2/AVTZ	2.30 <sup>a</sup>	1.96 <sup>a</sup>	178.7 <sup>a</sup>	2.60 <sup>a</sup>
2	B3LYP/AVTZ	2.34	2.03	175.3	2.63
	B971/AVTZ	2.33	2.02	175.8	2.66
	PBE0/AVTZ	2.31	2.01	175.0	2.59
	M06/AVTZ	2.33	2.02	175.8	2.58
	B3PW91/AVTZ	2.32	2.01	175.0	2.59
	MP2/AVTZ	2.31 <sup>a</sup>	1.97 <sup>a</sup>	176.5 <sup>a</sup>	2.47 <sup>a</sup>

<sup>a</sup> MP2 values from ref. [16]

**Table 2.** Calibration of the method: comparison of DFT vs. counterpoise-corrected MP2 incremental binding energies (kcal/mol) of the minimum-energy  $\text{HgClOH}-(\text{H}_2\text{O})_n$  ( $n=1, 2$ ) structures.

Method	$n=1$	$n=2$
B3LYP/AVTZ	6.23	11.45
B97-1/AVTZ	6.91	11.86
PBE0/AVTZ	7.11	12.40
M06/AVTZ	8.52	12.77
B3PW91/AVTZ	5.25	10.90
MP2/AVTZ	11.19	14.77
Counterpoise MP2/AVTZ <sup>a</sup>	6.45	11.95
MP2 CBS limit <sup>a</sup>	5.20	11.49

<sup>a</sup> From ref. [16].

With the optimized geometries, harmonic frequencies and water binding energies obtained with the various methods (all using the AVTZ basis sets), we determined the following RMS

errors with respect to the MP2/AVTZ references:

	B3LYP	PBE0	M06	B97-1	B3PW91.
RMS-geometries(Å)	0.51	0.55	0.35	0.42	0.59
RMS-frequencies( $\text{cm}^{-1}$ )	25.19	24.81	34.11	23.73	23.52
RMS-WBE(kcal/mol)	0.38	0.56	1.57	0.33	1.13
RMS-Total <sup>a</sup>	25.20	24.82	34.14	23.74	23.55

<sup>a</sup>Overall dimensionless measure defined as  $RMS = \sqrt{(RMS_{geom})^2 + (RMS_{freq})^2 + (RMS_{WBE})^2}$

We have thus employed the hybrid B3PW91 functional to perform the stepwise solvation study. In order to examine carefully the PES, we developed an exhaustive search of many possible solute-water configurations for  $n < 5$ . Consequently, the B3PW91/AVTZ optimized geometries obtained for the microsolvated HgClOH molecule up to the pentamer [HgClOH-(H<sub>2</sub>O)<sub>4</sub>] are in good agreement with the global minima reported previously at the MP2 level [16].

As mentioned above, in order to perform a systematic study of much larger clusters at the same level of theory, we have employed the 6-311G(d,p) basis sets for O and H to determine the structures and Gibbs free water binding energies of HgClOH-(H<sub>2</sub>O)<sub>*n*</sub> ( $n=1-24$ ) clusters. Gibbs free energies were calculated within the harmonic approximation at 298K. The geometries for a given  $n$  value were optimized using as starting points different positions and orientations of the hydrogen bonds that can be formed between the HgClOH-(H<sub>2</sub>O)<sub>*n-1*</sub> optimized geometry with the additional water molecule. Therefore, the free binding energies reported here are upper bounds to the true values for large  $n$ . All electronic calculations were performed with the Gaussian09 program [19]. In the following section we also discuss the effects of simulating a continuous solvent with the PCM scheme.

### B. DFT molecular dynamics

The thermal stability of the  $\text{HgClOH}-(\text{H}_2\text{O})_{24}$  fully solvated structure has been tested using a Born-Oppenheimer molecular dynamics (BO-MD) simulation at the B3PW91/6-311G\*\* level. This simulation was carried out *in vacuo* with the Geraldyn2.1 code based on the method developed by Raynaud *et al.* [20], which uses the velocity-Verlet integration scheme [21]. For the integration of the equations of motion a time step of 0.5 fs was used. A Nosé–Hoover chain of four thermostats [21,22] was used to control the temperature at 700K during the 10 ps of the simulation. Note that this temperature is higher than the critical point of water but it involves a rather small thermal energy of ca. 1.5 kcal/mol. The electronic structure DFT calculations involve 642 molecular orbitals and the total BO-MD simulation took 58 CPU days on 32 processors@2.8GHz running the Linux versions of Geraldyn2.1-G03.

### III. Results and discussion

#### *Stepwise solvation: B3PW91/AVTZ static results*

In table 3 we compare the static optimized geometrical parameters obtained at B3PW91/AVTZ level for the solute and the molecule solvated with one up to four water molecules with counterpoise-corrected MP2/AVTZ static values [16]. Previously obtained BO-MP2 dynamic averages are also given for the bare solute [24]. The B3PW91 Hg-Cl (2.31 Å) and Hg-OH (1.97 Å) distances of the isolated HgClOH molecule are in agreement with MP2 static [16] and dynamic [23] values. Note that both static models slightly overestimate (ca. 6°) the Cl-Hg-O angle compared to the dynamic MP2 average value (171°). Figure 1 shows the optimized structure for the solute.

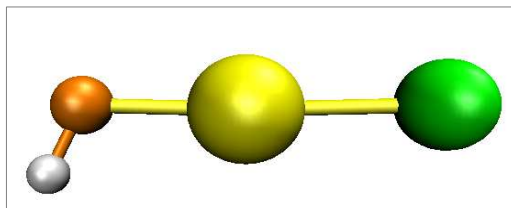


**Figure 1.** Optimized geometry of bare HgClOH.

**Table 3.** B3PW91/AVTZ optimized geometrical parameters of HgClOH-(H<sub>2</sub>O)<sub>n</sub> (*n*=1-4) complexes. B3PW91/6-311G\*\* values in parentheses. The O<sub>w</sub> stands for the water oxygen atoms directly linked to Hg. Distances in Å, angles in degrees.

Water molecules	Hg-Cl	Hg-O(H)	Cl-Hg-O(H)	Hg-O <sub>w</sub>	Hg-O <sub>w</sub>
0	2.31(2.34) 2.30 <sup>a</sup> 2.338 <sup>b</sup>	1.97(1.99) 1.94 <sup>a</sup> 2.001 <sup>b</sup>	177.0(176.6) 176.5 <sup>a</sup> 171.1 <sup>b</sup>		
1	2.31(2.34) 2.30 <sup>a</sup>	1.99(2.02) 1.96 <sup>a</sup>	179.7(178.8) 178.7 <sup>a</sup>	2.70(2.70) 2.60 <sup>a</sup>	
2	2.32(2.35) 2.31 <sup>a</sup>	2.01(2.04) 1.97 <sup>a</sup>	174.9(173.2) 176.5 <sup>a</sup>	2.61(2.53) 2.47 <sup>a</sup>	
3	2.33(2.36)	2.01(2.04)	173.6(170.8)	2.56(2.47)	
4	2.33(2.37)	2.03(2.07)	172.6(170.1)	2.94(2.53)	3.15(2.75)

<sup>a</sup>) Static MP2 values from ref. [16]

<sup>b</sup>) Dynamical MP2 average at 300K from ref. [24]

For *n*=1 and *n*=2 (see figure 2), we find that the B3PW91 optimized structures are consistent with those reported at the MP2 level [16]. The intra and inter-molecular distances at the DFT level are slightly larger in all cases, while the Cl-Hg-O(H) angle slightly oscillates depending on the *n* value. The first direct mercury-water interaction (2.70 Å) appears from the beginning of the solvation process with *n*=1.

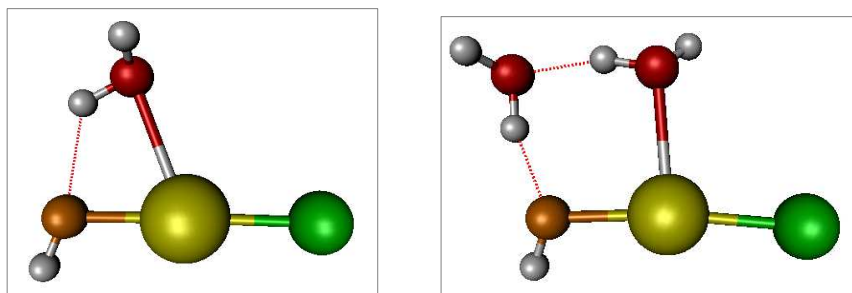


**Figure 2.** B3PW91 geometries of HgClOH solvated by one and two water molecules.

For  $n=3$  and  $n=4$  we found two slightly different minima when compared to those computed at the MP2 level [16] (see Figure 3). While the MP2 scheme predicts two direct water-Hg orbital interactions for  $n=3$ , the B3PW91 scheme favors the formation of two new hydrogen bonds between the water molecules. For  $n=4$  the difference with the MP2 optimized structure is qualitatively less important, since both the DFT and the *ab initio* methods yield two direct water-Hg orbital interactions, the latter also predicting the first hydrogen-halogen bridge. Therefore, for small  $n$  values, with this hybrid DFT method we find a faster evolution of the hydrogen bond network, mainly due to more significant contributions of the water-water interactions with respect to the water-mercury and water-halogen interactions.

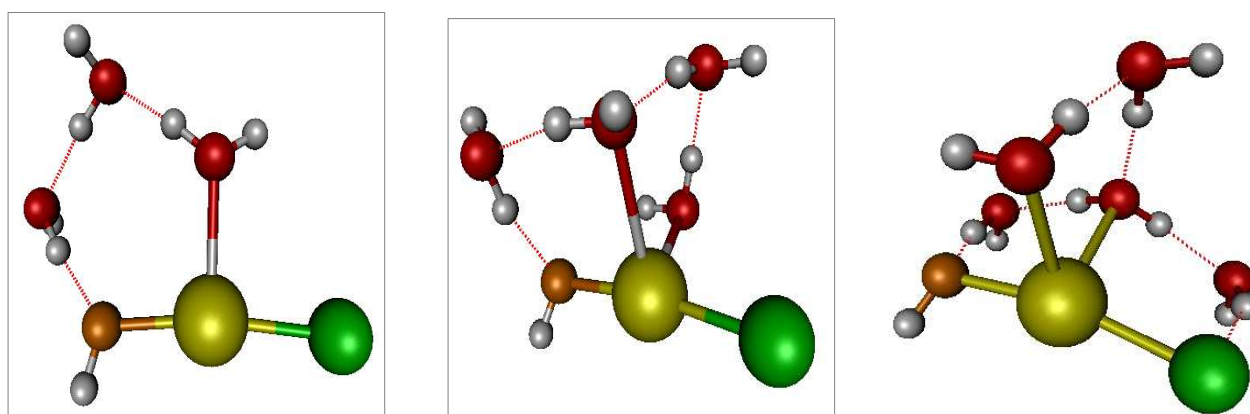


**Figure 3.** B3PW91 HgClOH geometries solvated by three, four and five water molecules.

In table 4 B3PW91/AVTZ incremental binding energies of the four  $n$  values are given. For comparison, B3PW91/6-311G\*\* and counterpoise-corrected (CC) MP2/AVTZ incremental

energies are also included. Note that, at this point, the entropic contributions are not taken into account. It is crucial to emphasize that the incremental energies (5.25 and 10.90 kcal/mol) computed with the B3PW91 scheme and the AVTZ basis sets are in excellent agreement with the counterpoise-corrected MP2 complete basis set values reported previously for  $n=1$  and 2 (5.20 and 11.49 kcal/mol). On the other hand, for  $n=3$  the presence of two new hydrogen bonds between the H<sub>2</sub>O molecules at DFT level gives rise to a slightly larger incremental binding energy value (8.16 kcal/mol) compared with the incremental CC-MP2 value (6.69 kcal). This trend is reversed when the fourth water molecule is added to the cluster. In that case, the structure computed at DFT level has a lower incremental binding energy (6.53 kcal/mol) than the CC-MP2 optimized value (10.01 kcal/mol) for the MP2. Here note that, while MP2 calculations considerably overestimate the interaction energies due to the basis set superposition error [16], the much faster B3PW91/AVTZ calculations directly lead to reasonably accurate incremental interaction energies even without the counterpoise correction. Note, however, that B3PW91/6-311G\*\* approach leads to overestimated values. So keeping in mind that the B3PW91 method provides an approximate description of the aqueous solvation for this metallic species, it is clear that the study of much larger clusters cannot be achieved at the MP2/AVTZ level. Therefore, we continue to address the study of larger clusters with the B3PW91/6-311G\*\* approach.

For the study of much larger HgClOH-(H<sub>2</sub>O)<sub>*n*</sub> clusters the oxygen and hydrogen atoms have been described with the 6-311G(d,p) basis sets. The evolution of the total Gibbs free water binding energies is presented in Figure 4. The corresponding data are given in table 2 of the Supplementary Material. Some interesting aspects can be observed. For instance, the absolute value of the incremental free energy for  $n=2$  (-1.94 kcal/mol) is nearly five times larger compared with the value for  $n=1$  (-0.40 kcal/mol), this suggests that the Hg-O(water) interaction plays a more important role in the trimer ( $n=2$ ) than in the dimer ( $n=1$ ) case, in

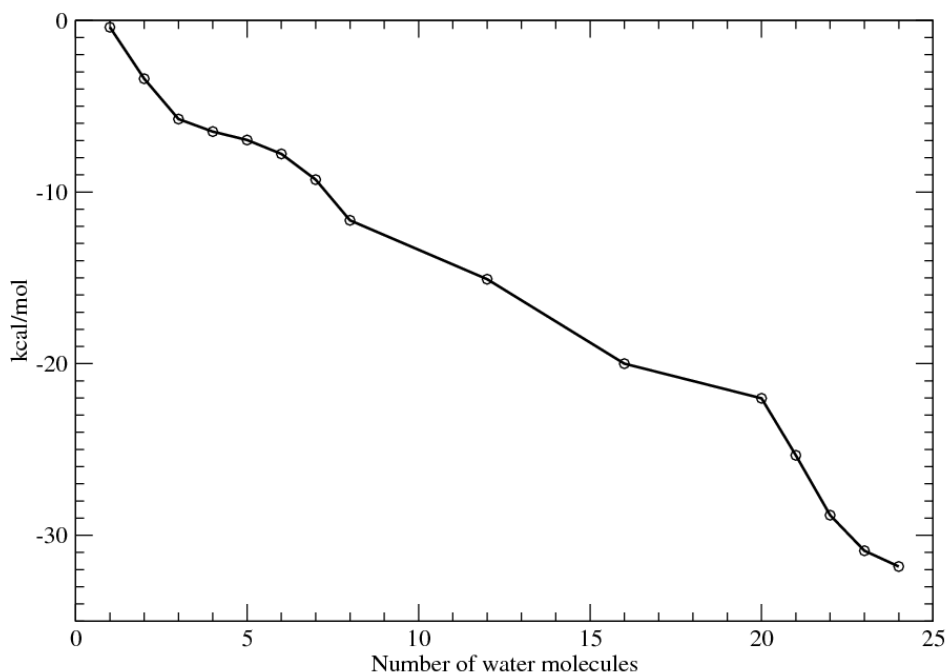
spite of the fact that the thermal correction to the Gibbs free energy for the trimer is much larger (16.9 vs. 2.9 kcal/mol) than for the dimer. This fact is also consistent with the shorter Hg-O<sub>w</sub> distance for the trimer than for the dimer, 2.5 vs. 2.7 Å, respectively .

**Table 4.** Comparison of B3PW91 vs. MP2 incremental binding energies (kcal/mol) at 0K of the minimum-energy HgClOH-(H<sub>2</sub>O)<sub>n</sub> (n=1-4) structures with AVTZ basis sets. B3PW91/6-311G\*\* values in parentheses.

<b>Theory level</b>	<b><i>n=1</i></b>	<b><i>n=2</i></b>	<b><i>n=3</i></b>	<b><i>n=4</i></b>
B3PW91/AVTZ	5.25 (10.80)	10.90 (15.83)	8.16 (12.53)	6.53 (13.34)
MP2/AVTZ	11.19	14.77	11.63	15.25
Counterpoise MP2/AVTZ <sup>a</sup>	6.45	11.95	6.69	10.01
MP2/CBS limit <sup>a</sup>	5.20	11.49	6.63	10.00

<sup>a</sup>From ref. [16]

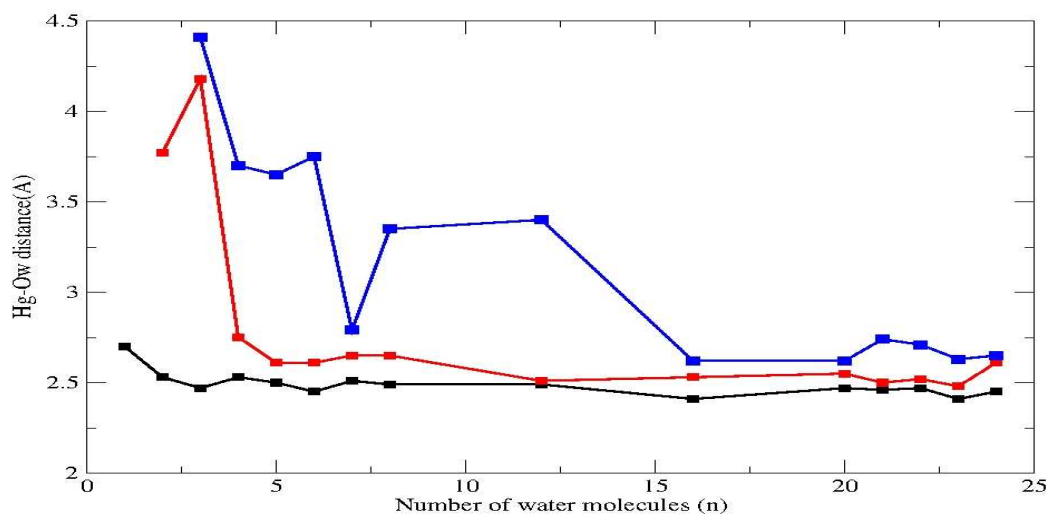
For n>20 note that the near-constant changes of 2-3 kcal/mol per additional water are consistent with the fact that the first solvation shell has been fully formed, i.e., that each additional water molecule simply builds new hydrogen bonds with water molecules that constitute the first solvation shell and have little effect on the internal “core” geometry of the cluster.



**Figure 4.** Gibbs free water binding energies vs. number of water molecules in  $\text{HgClOH}-(\text{H}_2\text{O})_n$  clusters.

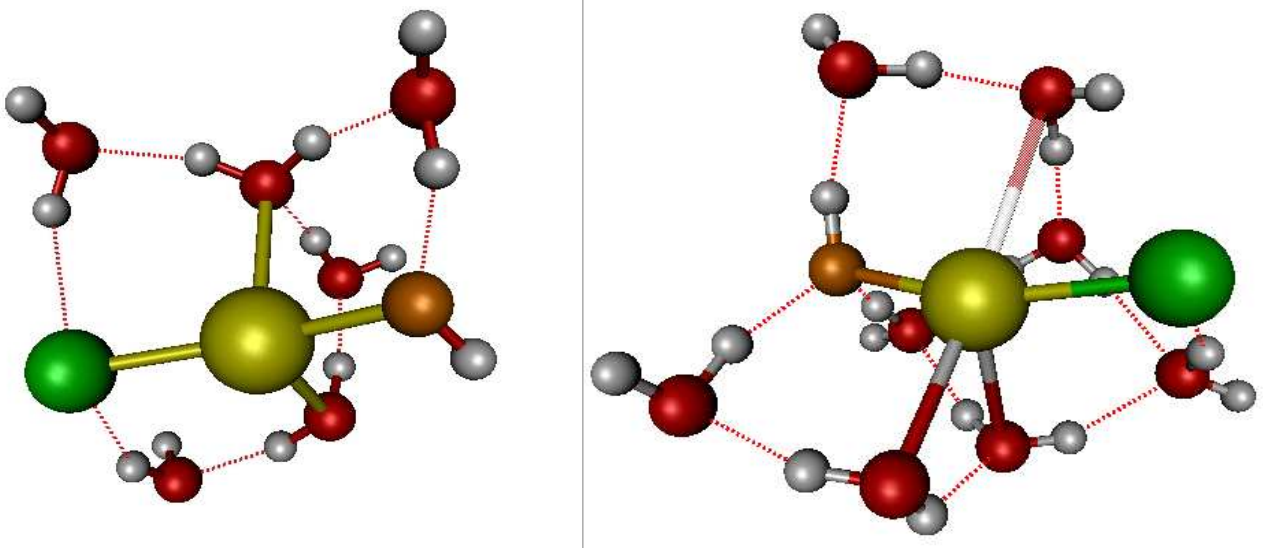
The main optimized geometrical parameters computed at the B3PW91/6-311G(d,p) level are presented in table 4 in the supplementary material. These parameters include the Hg-Cl, Hg-O(H) and the three shortest Hg-O<sub>w</sub> distances as well as the Cl-Hg-O(H) angle. As can be expected, the Hg-Cl and the Hg-O(H) distances slightly increase from 2.34 and 1.99 Å without solvation to 2.46 and 2.10 Å with 24 solvating water molecules, respectively. However, two noteworthy features appear. First, the solute Cl-Hg-O(H) angle shows large variations from the near-linear configuration (178° and 173°) with one and two water molecules, decreasing to 159° and 154° with  $n=6$  and 12, respectively. Secondly, while the shortest Hg-O<sub>w</sub> distance varies little with increasing number of water molecules (2.7 to 2.45 Å), the second and third Hg-O<sub>w</sub> distances show rather large variations, ranging from 3.77 and 4.4 Å with  $n=2$  and 3 to 2.61 and 2.65 Å with  $n=24$ . Figure 5 shows the evolution of the optimized shortest

Hg-O<sub>w</sub> distances vs. the number of water molecules. While the coordination of Hg with three equatorial water molecules appears with n=7 for the first time, we stress that the third water molecule still lies 2.8 Å from the Hg center.



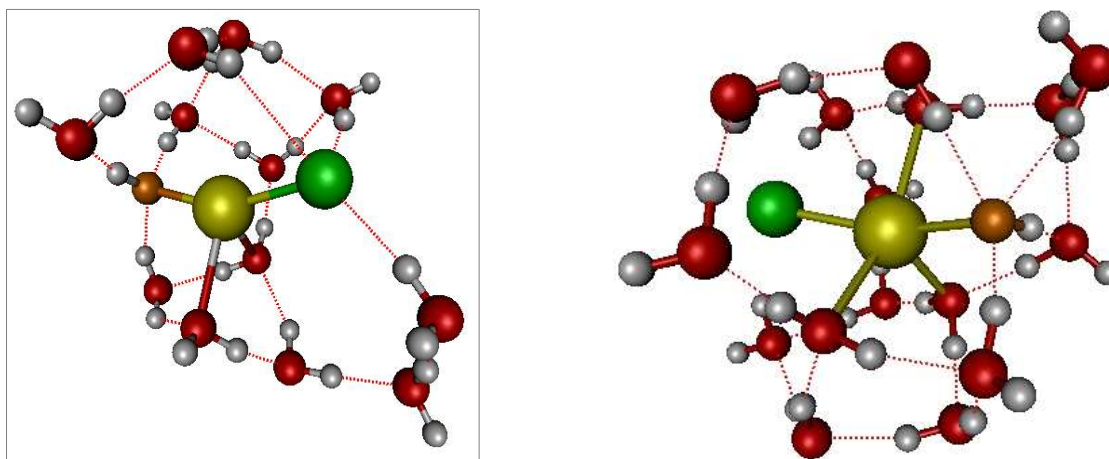
**Figure 5.** Hg-O<sub>w</sub> distance evolution for the oxygen atoms directly interacting with Hg.

Figure 6 shows the optimized geometries of HgClOH solvated by 6 and 8 water molecules, note that for the latter the third Hg-O<sub>w</sub> distance is even larger (3.35 Å)



**Figure 6.** Optimized geometries of HgClOH solvated by 6 and 8 water molecules.

Figure 7 shows the optimized geometries of the solute solvated by twelve and sixteen water molecules. Note the presence of three Hg–O<sub>w</sub> (water) direct interactions (2.41, 2.53 and 2.62 Å) leading to a close packed trigonal bipyramid pattern around Hg when  $n$  reaches 16 and this local solvation pattern remains for larger values of  $n$ .



**Figure 7.** Optimized geometries of HgClOH solvated by 12 and 16 water molecules

We found that 22 water molecules are needed to build the first solvation shell. When this point is reached, the addition of one extra water molecule has to be done by making two new hydrogen bonds with the previously existing water network, so that the 23<sup>rd</sup> water molecule is

not directly interacting with the HgClOH solute but merely serving as a water-water bridge. On the other hand, the optimized structure with 21 water molecules leaves a region around HgClOH without the effect of aqueous solvation, in other words, leading to an incomplete surface coverage of the solute by the solvent (see Figure 8).

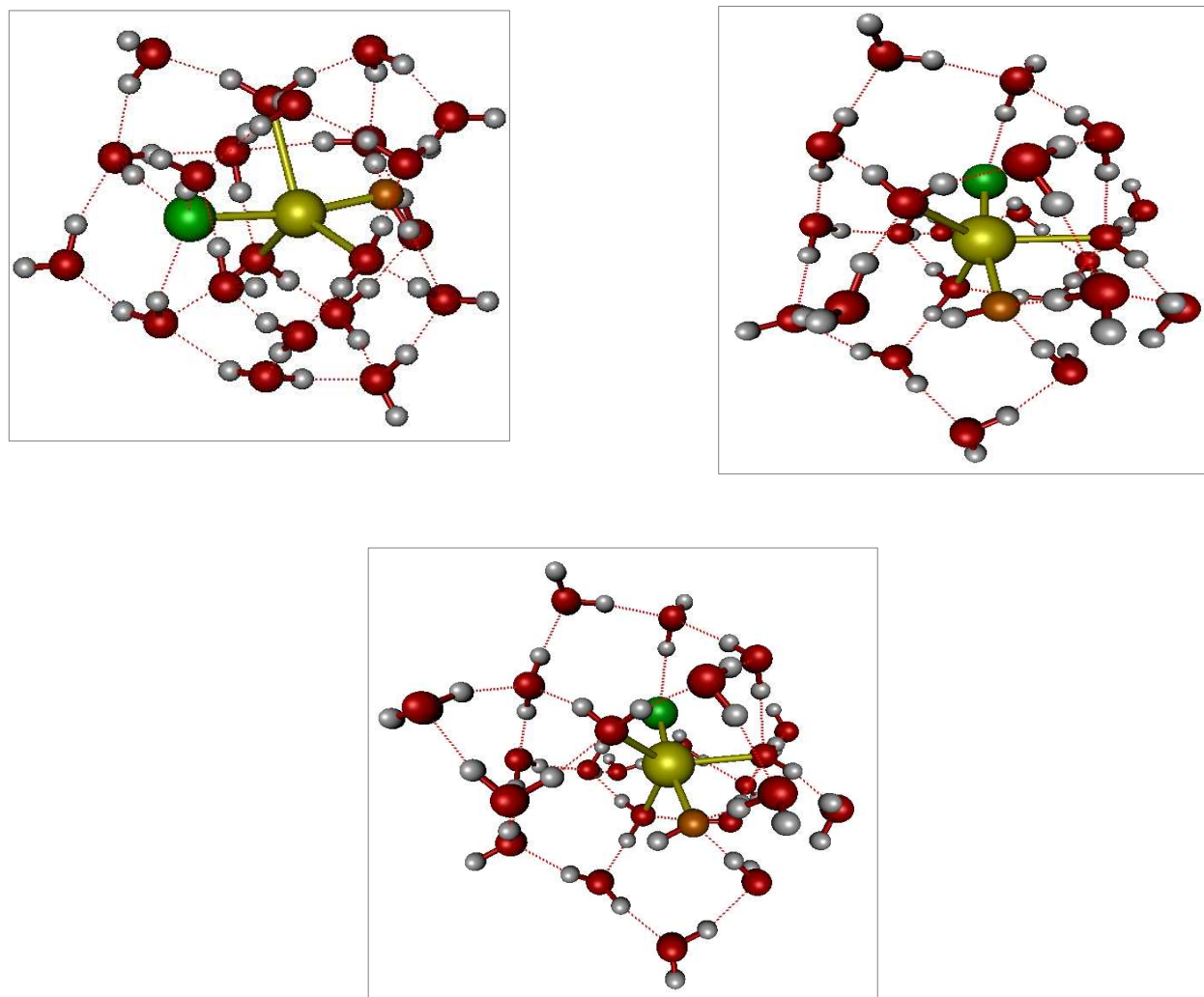


**Figure 8.** Optimized geometries of HgClOH solvated by 21,22, 23 water molecules.

The largest solvated complex we considered comprises 24 water molecules (figure 9). Note the *apical* coordination pattern where the Cl, Hg and O atoms of the solute recover a nearly-linear configuration; a similar coordination has been reported for  $\text{Hg}(\text{OH})_2\text{-(H}_2\text{O)}_{24}$  [9] and  $\text{HgCl}_2\text{-(H}_2\text{O)}_{24}$  [10]. We recall that Castro *et al.* [10], besides finding the apical structure, also

found a stable equatorial trigonal bipyramid pattern for the  $\text{HgCl}_2$  case. Therefore, we explored different configurations in order to find an equivalent solute-equatorial structure. However, only stable apical solvated structures were found having very similar (within 3 kcal/mol) Gibbs free energies; note that we present here only the one corresponding to the lowest Gibbs free energy (ca. -32 kcal/mol).

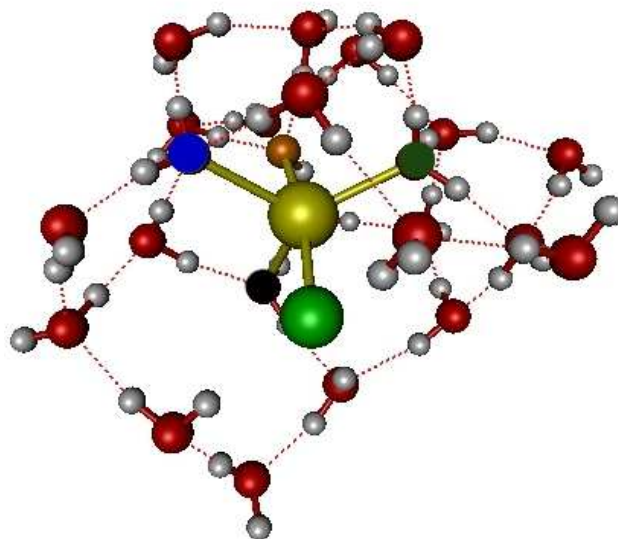


**Figure 9.** Optimized geometry of  $\text{HgClOH}$  solvated by 24 water molecules at 0K. We highlight the three water oxygens in the equatorial plane of the trigonal bipyramid (blue, dark green and black atoms) and the solute oxygen atom is shown in gold.

Figure 10 shows the evolution of the number hydrogen bonds as function of number of  $\text{H}_2\text{O}$  molecules in the network. Note a quasi linear dependence between these quantities. Based on a detailed analysis, on average, two new hydrogen bonds appear when each water molecule is added. This fact can be explained since we have not attained the bulk regime of the aqueous solution where, on average, each water has four (two donor and two acceptor) hydrogen bonds.

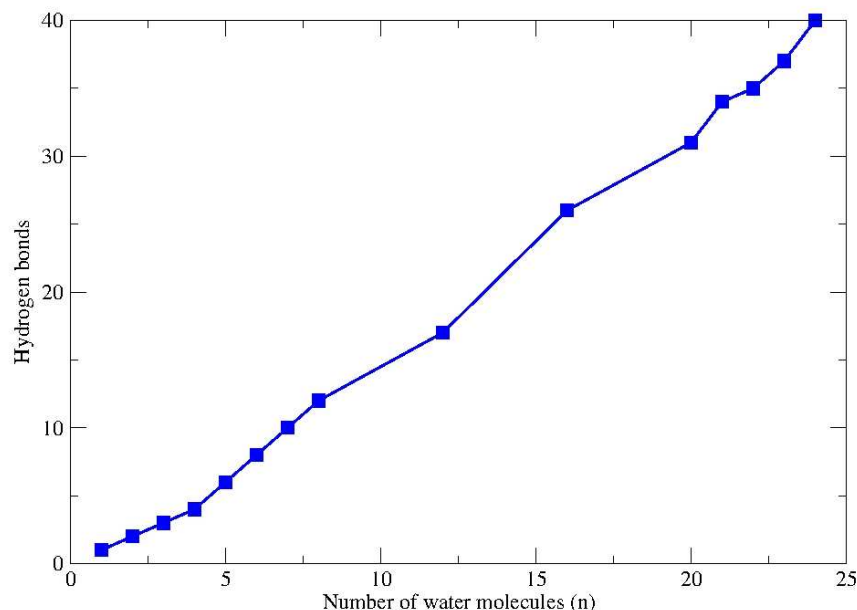


**Figure 10.** Hydrogen bonds vs. number of water molecules ( $n$ ) in  $\text{HgClOH}-(\text{H}_2\text{O})_n$  clusters. In order to address the possible effects of the polar aqueous medium on the geometry of the optimized structures including explicit water molecules we performed calculations using the Polarizable Continuum Model (PCM) of Tomasi *et al.* [25] as implemented in Gaussian09; we used the same 6-311G(d,p) basis sets as above. As is well known, in the PCM approach the solvent, in this case water, is represented by a continuous dielectric, which is characterized by its dielectric constant ( $\epsilon = 78.355$ ). Thus, we re-optimized the structures determined as minima *in vacuo* for selected values of  $n$ ; Table 3 in supplementary material shows the main geometrical parameters obtained *in vacuo* and their modified values obtained after re-optimization with the PCM scheme. It can be seen that the PCM optimized intermolecular distances are overestimated. For the bare the solute intramolecular Hg-Cl and Hg-O(H) PCM distances are 0.1 and 0.06 Å longer. However, when explicit water molecules are considered, the overestimation of the Hg-O<sub>w</sub> distances is surprisingly large, especially for the smaller clusters. To emphasize this, note that for  $n=1, 2, 3, 6,$  and  $12$  the differences with the shortest optimized B3PW91 Hg-O<sub>w</sub> distances are 1.19, 1.03, 1.02, 1.36 and 0.45 Å, respectively. It is

clear that the PCM scheme significantly favors the separation of the explicit water molecules from the solute, leading to a rather loosely bound solvating water network around HgClOH in a clathrate manner. As an example of this, table 4 in the Supplementary Material shows the vibrational frequencies obtained for the optimized B3PW91/6-311G\*\* HgClOH-H<sub>2</sub>O complex *in vacuo* and with the PCM scheme with water as continuous solvent. Note that the largest relative changes in frequency with the PCM scheme appear in two cases: for the mode coupling the H-O-Hg-O<sub>w</sub> dihedral of the water oxygen to HgClOH (46 cm<sup>-1</sup> in 207 cm<sup>-1</sup>) and, for the O-H stretching (the intermolecular H-bond) mode of the solvating water molecule (-327 cm<sup>-1</sup> in 3717 cm<sup>-1</sup>). Figure 11 presents the B3PW91-PCM optimized geometry for the HgClOH-(H<sub>2</sub>O)<sub>1,3</sub> cases, where the closest Hg-O<sub>w</sub> distances are 3.89 and 3.49 Å vs. 2.69 and 2.47 Å obtained *in vacuo*. For the HgClOH-(H<sub>2</sub>O) PCM case we stress the total absence of orbital interaction between Hg and the water oxygen, clearly showing that the O<sub>w</sub> lone pair solvation by the PCM scheme is energetically more favorable than the interaction with Hg. For the latter note the very loosely bound water structure around HgClOH as compared with the one shown in figure 3 (left).

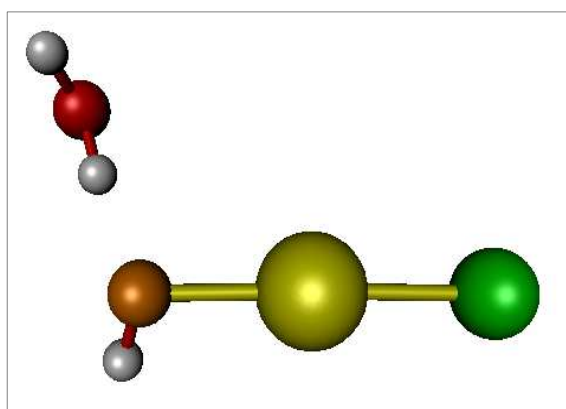
Let us now focus on the energetic aspect of the PCM results. Table 5 shows the values of the Gibbs free energies at 298K of the solute, of a single water molecule and of the optimized structures for selected *n* values, both *in vacuo* and in the polarizable medium with PCM. For *n*=0, the difference of the Gibbs free energy *in vacuo* and in the polarizable medium is -38.8 kcal/mol, which provides an approximation to the solvation energy of this species in water. Here we have employed the usual definition of the incremental water binding energies [17], i.e.,  $\Delta G^\circ = [G^\circ(\text{HgClOH with } n \text{ water molecules}) - nG^\circ(\text{H}_2\text{O}) - G^\circ(\text{HgClOH})]$ . One might be tempted to obtain the incremental water binding energies for *n*>0 considering the polarizable medium. However, it can be easily shown that incremental water binding energies obtained with the PCM approach are fundamentally wrong for a simple reason. First of all, note that the

continuous solvent model leads to a nearly constant decrease of the Gibbs free energies of ca. 0.06 a.u. for all  $n$ , roughly corresponding to the solvation energy of the bare solute. This fact is explained by the near-constant increase in the size of the surface which defines the solute cavity since, with each additional water molecule considered as solute, three new spheres (one with the oxygen atom radius and two with hydrogen radii) are added to the cavity generation algorithm of the PCM code.

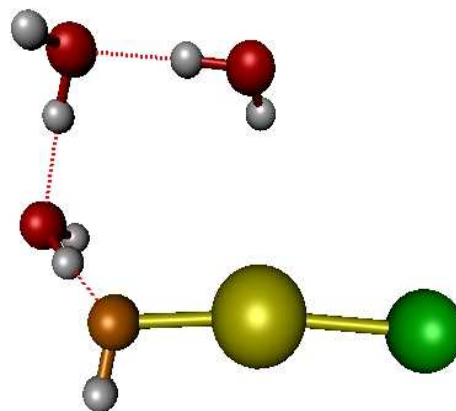
Secondly, the sum of the Gibbs free energy of the fragments, HgClOH plus  $n$  times that of an isolated water in the PCM scheme is obviously more negative than that of the HgClOH-(H<sub>2</sub>O) <sub>$n$</sub>  complex. Note that this difference becomes even larger for larger  $n$ , thus suggesting that these complexes never get to form. This is so because the polarizable medium solvation of the isolated water molecules (or even of the frozen-geometry -(H<sub>2</sub>O) <sub>$n$</sub>  water clusters derived from the optimized HgClOH-(H<sub>2</sub>O) <sub>$n$</sub>  structures), with the PCM approach always leads to lower energies due to the larger surface area of the separated fragments. This is the fundamental reason why previous studies on explicit aqueous microsolvation of mercury mono and dihalides [17] as well as of thiosulfuric acid and its tautomeric anions [26] did not address the energetic differences with the polarizable medium model. We emphasize once again that incremental water binding energies cannot be interpreted as incremental solvation energies since, with increasing  $n$  values, they include the water-water attractive interactions which are not directly related to the stabilization of the solute by the presence of the neighboring aqueous environment.

**Table 5.** Gibbs free energies (a.u.) at 298K for selected  $\text{HgClOH}-(\text{H}_2\text{O})_n$  optimized structures. Values in parentheses correspond to those obtained with the PCM scheme for liquid water.

$\text{HgClOH}-(\text{H}_2\text{O})_n$ $n$	$G^0_{298}(\text{B3PW91/6-311G}^{**})$	
0	-244.452963	(-244.514911)
1	-320.875566	(-320.939438)
2	-397.289929	(-397.353105)
3	-473.708910	(-473.771449)
6	-702.952377	(-703.023633)
12	-1161.464962	(-1161.532008)
$\text{H}_2\text{O}$	-76.415041	(-76.422404)



a)



b)

**Figure 11.** Optimized B3PW91 geometries of the  $\text{HgClOH}-\text{H}_2\text{O}$  (a) and  $\text{HgClOH}-(\text{H}_2\text{O})_3$  (b) complexes with the PCM scheme for water as a continuous solvent. Note the total absence of  $\text{Hg}-\text{O}_w$  interaction in the first case and the much longer  $\text{Hg}-\text{O}_w$  distance in the latter as compared with the structure in figure 3.

Before passing to the dynamical results we point out that we tried to address the effects of dispersion-corrected density functionals on structures and energies. Disappointingly we found that no quantum chemistry program available to us (Gaussian09, Molpro-2010, NWChem or CRYSTAL) is capable of using dispersion-corrected density functionals for mercury containing molecules. However, at this point we recall that, while the M06 functional was not only designed to account for dispersion corrections it partially accounts for these effects; the comparison of the M06 and the *ab initio* MP2 results described earlier in this study indicate that there are small differences with the B3PW91 ones, suggesting that dispersion effects are small on the presently optimized  $\text{HgClOH}(\text{H}_2\text{O})_n$  complexes.

#### *DFT Born-Oppenheimer molecular dynamics simulation*

To address the role of thermal effects on the fully solvated structure, a Born–Oppenheimer MD simulation at the B3PW91 level part of that high temperature (700 K) was carried out. As previously done for  $\text{HgCl}_2$  [10], the simulation started from the  $\text{HgClOH}(\text{H}_2\text{O})_{24}$  optimized structure with random velocities consistent with the fixed temperature. A particularly important feature of the dynamical results is the stability of the cluster-derived first solvation shell. Throughout the MD simulation we observed the persistence of a trigonal bipyramid coordination pattern around Hg, as shown by the representative geometry depicted in Figure 12. Note however that up to seven water molecules actively participate in setting up of this pattern throughout the simulation. This BO-MD simulation allows us to examine the evolution of the main geometrical parameters, in particular, the behavior of intermolecular Hg-O(water) distances.

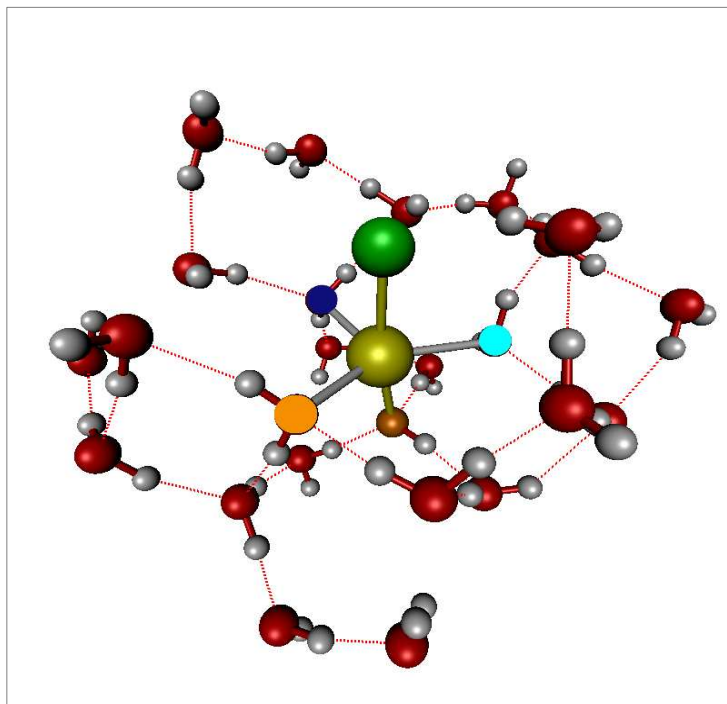


**Figure 12.** Representative geometry of HgClOH solvated by 24 water molecules with BO-DFT-MD simulation at 700K. We highlight the three oxygens that directly interact with the mercury (blue, orange, turquoise) during the simulation. The solute oxygen atom is shown in gold.

Figure 13 shows the Hg-O<sub>w</sub> distance evolution for the seven water oxygens that directly interact with mercury during the BO-MD simulation as well as the solute Cl-Hg-O angle. Note that the first water exchanges, occurring very early ( $t < 0.8$  ps) in the simulation, take out two of the equatorial water molecules (black and green curves) and these molecules never come back to interact directly with Hg again. On the other hand, exactly the opposite happens for a water molecule (orange curve) whose optimal distance is far from Hg and, after around 1ps comes into the trigonal equatorial coordination around Hg to remain there until the end of the simulation. Intermediate situations are found, where two water molecules (pink and light blue curves) originally not coordinated to Hg, intermittently build up the trigonal coordination environment around Hg. Only one (purple curve) of the seven closest water molecules briefly participates in the formation the trigonal coordination environment around Hg; it quickly

approaches Hg while another molecule (light blue curve) recedes from Hg due to steric impediments, to finally move away (all this in less than 0.4 ps). However, we emphasize that after 5 ps the Hg-O<sub>w</sub> oscillations become smaller and the number of water exchanges decreases due to thermalization. Therefore, using the last 5 ps of the simulation we can roughly estimate that one water exchange takes place every 10 ps after thermalization has been achieved. This  $10^{11} \text{ s}^{-1}$  rate can be compared with the water exchange rate in the first solvation shell of metal ions in aqueous solution. For instance, in the case of the bare Cs<sup>+</sup> ion the mean lifetime is 200 ps [28]. As could be expected, the much shorter lifetime we estimate here for molecules in the first solvation shell is in agreement with the smaller interaction energy of water with the neutral HgClOH molecule as compared to that of the ion-water system. However, we stress that: a) much longer simulation times would be needed to extract statistical data to determine a reliable average water-exchange period and, b) these mean lifetimes apply to gas-phase clusters and all the many body effects arising from the second and subsequent hydration shells are absent in this type of simulations. A summary of average values extracted from the last 5 ps of the simulation (after the thermalization period was achieved) is found in Table 6.

**Table 6.** Average of selected interatomic distances (Å) for HgClOH-(H<sub>2</sub>O)<sub>24</sub> calculated with the last 5 ps of the BO-MD simulation at 700 K. The blue, orange, turquoise, pink, dark green, purple, and black values correspond to the oxygen atoms highlighted in figure 12.

Hg-Cl	Hg-O(H)	Cl-Hg-O(H) angle/°	Hg-O <sub>Blue</sub>	Hg-O <sub>Orange</sub>	Hg-O <sub>Turquoise</sub>	Hg-O <sub>Pink</sub>	Hg-O <sub>Green</sub>	Hg-O <sub>Purple</sub>	Hg-O <sub>Black</sub>
2.47	2.10	168.7	2.58	2.61	2.74	4.15	3.86	3.92	4.34

The dynamical description provides similar Hg-Cl, Hg-O(H) and Cl-Hg-O average values (2.47 Å, 2.10 Å and 168.7°) compared with the static (2.46 Å, 2.10 Å and 170.0°) B3PW91/6-

311G\*\* values. The temporal evolution of the Cl-Hg-O angle of the solute throughout the simulation is shown in Figure 13b. The presence of chlorine atom produces a slight decrease on the angle average value ( $168.7^\circ$ ) compared with the  $\text{Hg}(\text{OH})_2$  case ( $171.1^\circ$ ) [9], where two hydroxyl groups are present. On the other hand, note that large amplitude oscillations ( $> 18^\circ$ ) occur between 1.5-2.0, 2.7-4.0 and 6.2-7.5 ps.

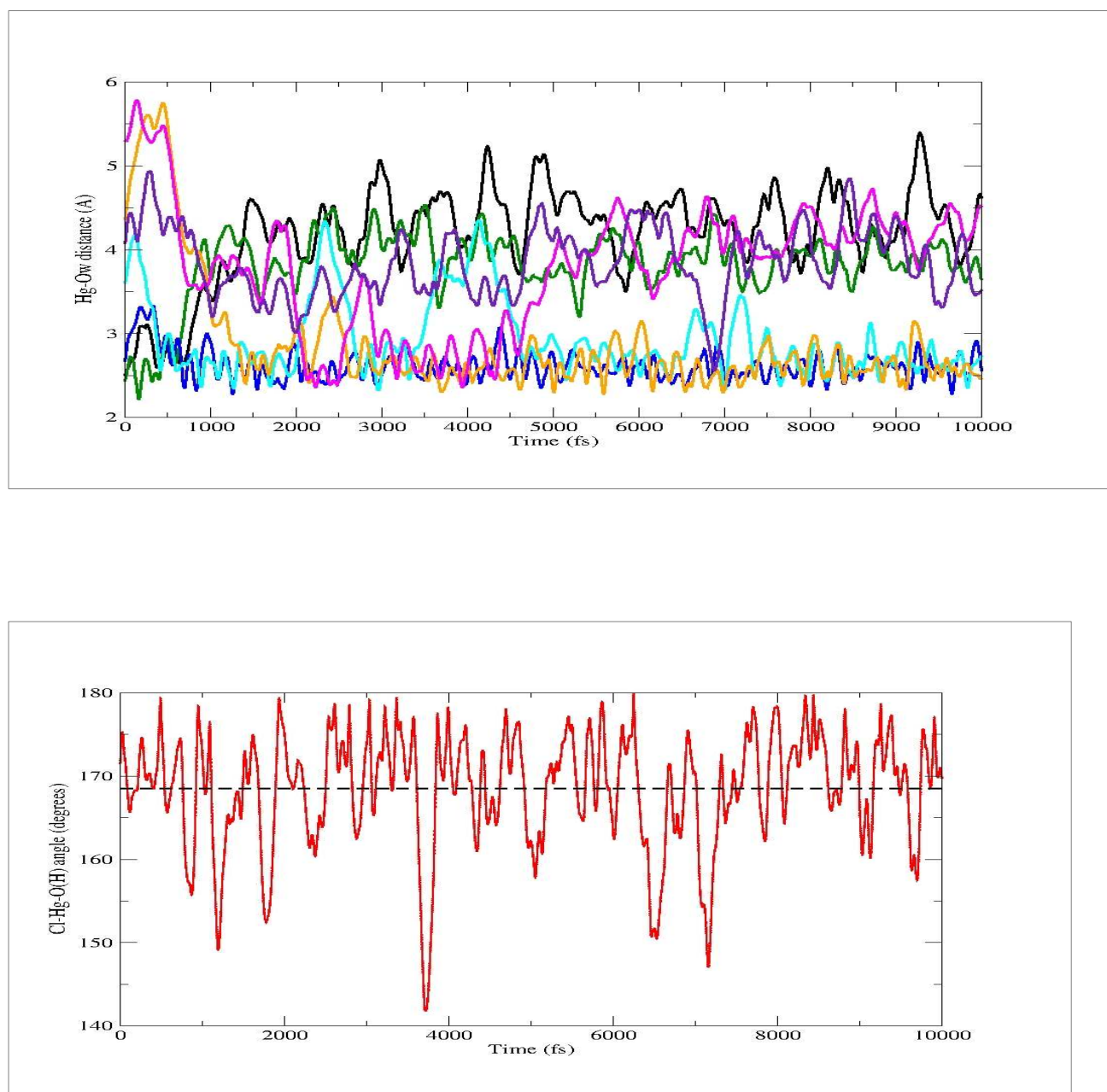


**Figure 13** Hg-O<sub>w</sub> distance evolution for the oxygen atoms directly interacting with Hg during the BO-MD simulation. Lower panel, solute Cl-Hg-O(H) angle evolution and the average value (dashed line) at T= 700K.

Finally, inspection of the dynamical simulation reveals that 17 out of 24 water molecules never get to participate in the coordination around Hg, simply breaking and making inter-water hydrogen bonds.

#### IV. Conclusions and perspectives

We have addressed the aqueous solvation of HgClOH using a cluster stepwise hydration scheme at the DFT level. We have shown that single-reference methods are well adapted to describe the HgClOH-(H<sub>2</sub>O)<sub>n</sub> systems through the evaluation of the T1Diagnostic at the CCSD/cc-pVTZ level of theory for the n=0,1 and 2 cases. In order to choose a suitable exchange-correlation functional, a careful calibration of key structural and energetic properties obtained with various functionals was done using MP2/AVTZ results as references for the smaller systems (n=0,1,2). This calibration showed, as found previously for the HgCl<sub>2</sub> and Hg(OH)<sub>2</sub> cases, that the B3PW91 functional yields the best performance overall. Therefore, at the B3PW91/6-311G\*\* level, we have obtained total and incremental water binding free energies, optimized geometries and Hg-coordination patterns of the HgClOH-(H<sub>2</sub>O)<sub>n</sub> complexes with  $n = 1-24$ .

We found that 22 water molecules are necessary to fully form the first solvation shell around HgClOH. For small  $n$  DFT energetic and structural optimized parameters are in close agreement with previous counterpoise-corrected MP2 calculations [16]. The water binding free energies are similar in magnitude to those found for the HgCl<sub>2</sub>-(H<sub>2</sub>O)<sub>n</sub> systems. After the first solvation shell is fully formed, 2-3 kcal/mol are gained with each additional water molecule. The intramolecular Hg-O and Hg-Cl solute distances practically remain unchanged along the solvation process, however the Cl-Hg-O angle of the solute shows a larger dependence with the  $n$  value. Three short Hg-O(water) orbital-driven equatorial interactions appear from  $n=16$  onwards. The pentacoordinated HgClOH trigonal bipyramid coordination

around Hg resembles those found in the microhydration patterns for  $\text{Hg}(\text{OH})_2$  [9] and  $\text{HgCl}_2$  [10] species. On average, two new hydrogen bonds appear when a new water molecule is added to the network, even for the larger clusters.

When considering the effects of a continuous polarizable solvent through the PCM scheme, the optimized geometries lead to very large Hg- $\text{O}_w$  distances due to the larger stabilization produced by the continuum solvation of the explicit water molecules. For the larger clusters the PCM optimized structures show a loosely bound water network around  $\text{HgClOH}$ , in a clathrate-like manner. The role of dispersion-corrected density functionals could not be assessed for these mercury-containing systems. However, comparison of the B3PW91 geometries and water binding energies with the MP2 and M06 results for small  $n$  suggest that the dispersion corrections to them should actually be small.

One important result is that, through a DFT Born-Oppenheimer-MD simulation, we have shown the thermal stability of the  $\text{HgClOH}(\text{H}_2\text{O})_{24}$  structure at temperatures as high as 700 K. Throughout the simulation we found a clathrate-like structure where the intra-molecular Hg-Cl and Hg-O(H) distances are slightly larger than the static optimized values. In the course of the MD simulation we observed several water exchanges, all of them in the equatorial plane. Nevertheless, the trigonal bipyramid structure around Hg remains as a stable motif throughout the simulation. After thermalization of the cluster is achieved, the exchange rate for the Hg-coordinated water molecules is estimated at around  $10^{11} \text{ s}^{-1}$ .

We emphasize that these static and dynamical descriptions of the first solvation shell of Hg-containing species using a stepwise hydration scheme yield a restricted view when compared with the full solvation that occurs in the liquid phase, however, they represent a crucial step in order to obtain a better description of the aqueous solvation through Monte Carlo simulations of the condensed phase. In this way, key structural and energetic data obtained in this study will be used to develop sophisticated MCDHO [27] classical interatomic refined potentials

needed to describe the energetic and structural properties of HgClOH in the condensed phase, as previously done for HgCl<sub>2</sub> [12].

### Acknowledgments

The authors thank support from the ECOS-ANUIES/CONACYT Mexican-French cooperation program through project M10-P01. AEJI thanks a graduate scholarship from CONACYT. LM is member of the Institut Universitaire de France. CINES and CalMiP are acknowledged for generous grants of computing time. LM is also grateful to the A. von Humboldt foundation. ARS also thanks CONACYT through the Basic Science project No. 130931 and for sabbatical support from the Professeur Invité program at INSA-Toulouse. This work was also supported by Programme Investissements d'Avenir under the program ANR-11-IDEX-0002-02, reference ANR-10-LABX-0037-NEXT.

### References

- [1] Gray, J. E.; Hines, M. E. *Appl. Geochem.* **2006**, 21, 1819-1820.
- [2] *Arctic Pollution 2011, Arctic Monitoring and Assessment Programme (AMAP)*, Oslo, **2011**.
- [3] Fitzgerald, W. F.; Mason, R. P. *Mercury and its effects on environment and biology*; 1st ed. Marcel Dekker, Inc.: New York, N.Y. **1997**, 34, 53–111.
- [4] Kim, K. H.; Hanson, P. J.; Barnett, M. O.; Lindberg S. E. *Mercury and its effects on environment and biology*; 1st ed. Marcel Dekker, Inc. New York, **1997**, 185.
- [5] Morel, F. M. M.; Kraepiel, A. M. L.; Amyot, M. *Annu. Rev. Ecol. Syst.* **1998**, 29, 543.
- [6] Larose, C.; Dommergue, A.; De Angelis, M.; Cossa, D.; Averty, B.; Maruszczak, N.; Soumis, N.; Schneider D.; Ferrari, C. *Geochim. Cosmochim. Acta*, **2010**, 74, 6263.
- [7] Gutknecht, J. *J. Membr. Biol.* **1981**, 61, 61.
- [8] Myers, G.J.; Davidson, P.W.; Cox, C.; Shamlaye, C.F.; Palumbo, D.; Cernichiari, E.; Sloane-Reeves, J.; Wilding, G.E.; Kost, J.; Huang, L.S.; Clarkson, T.W. *Lancet*, **2003**, 361, 1686.
- [9] Amaro-Estrada J.I.; Maron L.; Ramírez-Solís, A. *J. Phys. Chem. A* **2013**, 117, 9069–9075.

- [10] Castro, L.; Dommergue, A.; Renard, A.; Ferrari, C., Ramírez-Solís, A.; Maron, L. *Phys. Chem. Chem. Phys.* **2011**, 13, 16772-16779
- [11] Hernández-Cobos, J.; Vargas, M. C.; Ramírez-Solís, A.; Ortega-Blake, I. *J. Chem. Phys.* **2010**, 133, 114501.
- [12] Hernández-Cobos, J.; Ramírez-Solís, A.; Maron, L.; Ortega-Blake, I. *J. Chem. Phys.* **2012**, 136, 014502.
- [13] Dunning T. H. *J. Chem. Phys.* **1989**, 90, 1007.
- [14] Kuechle W.; Dolg M.; Stoll H.; Preuss H. *Mol. Phys.* **1991**, 74, 1245.
- [15] Bergner A.; Dolg M.; Kuechle W.; Stoll H., Preuss H. *Mol. Phys.* **1993**, 80, 1431.
- [16] Amaro-Estrada J. I.; Ramírez-Solís A. *Comput. Theor. Chem.* **2013**, 1006, 45.
- [17] B.C. Shepler; A.D. Wright; N.B. Balabanov; K.A. Peterson, *J. Phys. Chem. A* **2007**, 111, 11342
- [18] Reed, A.E.; Curtiss. L.A.; Weinhold, F. *Chem. Rev.* **1998**, 88, 899.
- [19] Frisch, M.J.; Trucks, G.W.; Schlegel, H.B.; Scuseria, G.E.; Robb, M.A.; Cheeseman, J.; Zakrzewski, V.G.; Montgomery, J.A.; Stratman, R.E.; Burant, J.C.; *et al. Gaussian 09*, Gaussian, Inc., Pittsburgh PA, **2009**.
- [20] Raynaud, C.; Maron, L.; Daudey, J.P. ; Jolibois, F. *Phys. Chem. Chem. Phys.* **2004**, 6, 4226.
- [21] Verlet, L. *Phys. Rev.* **1967**, 159, 98.
- [22] Nosé, S. *J. Chem. Phys.* **1984**, 81, 511.
- [23] Hoover, W.G. *Phys. Rev. A* **1985**, 31, 1695.
- [24] Ramírez-Solís, A.; Maron, L. *Int. J. Quant. Chem.* **2012**, 112, 3484.
- [25] Tomasi, J.; Cammi, R.; Mennucci, B.; Cappelli, C.; Corni, S. *Phys. Chem. Chem. Phys.* **2002**, 4, 5697.
- [26] R. Steudel and Y. Steudel, *J. Phys. Chem. A* **2009**, 113, 9920.
- [27] Saint-Martin H.; Hernández-Cobos J.; Bernal-Uruchurtu M.I.; Ortega-Blake I.; Berendsen H.J.C. *J. Chem. Phys.* **2000**, 113, 10899.
- [28] L. Helm and A.E. Merbach, *Coord. Chem. Rev.* **1999**, 187, 151.

## Graphical abstract

